AIAA JOURNAL
Vol. 45, No. 10, October 2007

Optimization Strategy for Minimizing Damage in Postbuckling Stiffened Panels

Andrea Faggiani* and Brian. G. Falzon†
Imperial College London, London, SW7 2AZ England, United Kingdom

DOI: 10.2514/1.26910

Composite materials are finding increasing use on primary aerostructures to meet demanding performance targets while reducing environmental impact. This paper presents a finite-element-based preliminary optimization methodology for postbuckling stiffened panels, which takes into account damage mechanisms that lead to delamination and subsequent failure by stiffener debonding. A global–local modeling approach is adopted in which the boundary conditions on the local model are extracted directly from the global model. The optimization procedure is based on a genetic algorithm that maximizes damage resistance within the postbuckling regime. This routine is linked to a finite element package and the iterative procedure automated. For a given loading condition, the procedure optimized the stacking sequence of several areas of the panel, leading to an evolved panel that displayed superior damage resistance in comparison with nonoptimized designs.

Nomenclature

$E_{11\text{compression}}$	=	longitudinal compressive modulus
$E_{11\text{tension}}$	=	longitudinal tensile modulus
$E_{22\text{compression}}$	=	transverse compressive modulus
$E_{22\text{tension}}$	=	transverse tensile modulus
f_i^m	=	ply-identity variable for −45- deg ply
f_i^p	=	ply-identity variable for 45-deg ply
G_{IC}	=	mode-I fracture toughness
G_{12}	=	in-plane shear modulus
$G_{\text{IIC}}/G_{\text{IIIC}}$	=	modes-II/III fracture toughness
n_i	=	ply-identity variable for 90-deg ply
o_i	=	ply-identity variable for 0-deg ply
ν_{12}	=	in-plane Poisson's ratio
$\sigma_{0\text{I}}$	=	maximum allowable traction (in mode I)
$\sigma_{0\text{II}}/\sigma_{0\text{III}}$	=	maximum allowable traction (in modes II/III)

I. Introduction

EFFECTIVE use of composite materials is revolutionizing the way aircraft and spacecraft structures are designed. Composite materials are ideal for structures that require high strength-to-weight and stiffness-to-weight ratios, and superior life-cycle costs can be achieved by taking advantage of their potential low maintenance. In particular, a lot of research effort is being spent on developing all-composite aerostructures for large military and civil transport aircraft. Current composite design tends to be conservative for primary structures under predominantly compressive loads. Fuselage panels and upper wing skins are examples of stiffened panels that are susceptible to buckling. The reluctance to fully exploit the postbuckling strength of stiffened composite panels stems from the susceptibility of a relatively weak skin-stiffener interface to through-thickness stresses arising from deformations due to buckling. To fully exploit the potential of this material in aerostructures, accurate knowledge of a structure's postbuckling behavior must be achieved.

Received 31 July 2006; revision received 22 May 2007; accepted for publication 15 June 2007.

*Ph.D. Researcher, Department of Aeronautics, South Kensington Campus.

†Reader in Advanced Aerostructures, Department of Aeronautics, South Kensington Campus (Corresponding Author).

The majority of experimental investigations into the buckling and postbuckling behavior of composite-stiffened panels involved loading the panels in uniaxial compression and observing their structural behavior before, during, and after buckling. This was done in tests conducted on graphite-epoxy hat- and blade-stiffened panels loaded in uniaxial compression, altering geometric parameters such as stringer sizing [1], and a variety of other panel configurations [2–4]. More recent work looked at the postbuckling behavior of a blade-stiffened composite panel loaded in uniaxial compression [5] and compared the structural response to other stiffened panels previously tested with hat-, I-, or J-shaped stiffeners [6–9].

Much of these experimental programs also addressed the failure modes of the panels tested. These indicated that failure was related to the initiation and progression of debonding of the skin from the stiffener at regions of the panel corresponding to buckle node and antinode lines. This occurs because of the nature and magnitude of the stresses that develop at the interface between the skin and stiffeners of the panel at these particular locations [8].

Work relating to optimization of composite structures originated from optimization of simple plate structures [10–18] and then evolved to more complex panel optimizations. This included work relating to an extensive optimization procedure for composite panels stiffened by stringers or rings and subjected to combined in-plane loads using the PANDA2 computer code to find minimum-weight designs for three different load cases and subject to various constraints [19].

When optimization involves the presence of integer variables such as the orientation of plies in composite structures, genetic algorithms (GAs) [20] have proven advantageous. A GA was tested [21] for maximizing the buckling load of a fixed-thickness laminate. This was then improved [22] and coupled with specific failure constraints [23] to optimize a design for minimum thickness and hence weight. The minimum-weight design of compressively loaded composite plates and composite-stiffened panels under constrained postbuckling strength has also been investigated [24], for which a nonlinear finite element (FE) analysis was used with a GA for the optimization process. Further work regarding GAs dealt with implementing new and improved genetic operators to improve and speed up their convergence to an optimum design [25–29].

To reduce the computational cost of GAs, a new approach was implemented in which a system of neural networks was set up and trained to "replace" the nonlinear FE analyses used to evaluate the panel's structural response [30]. To optimize stiffened composite panels for use in the postbuckling regime, a GA was then implemented. New improvements to the preceding method, incorporating strength constraints, were then investigated and applied to various optimization scenarios [31].

A limitation of the optimization procedures discussed is that they do not account for failure mechanisms that may occur before overall buckling collapse or in-plane structural failure. These mechanisms are primarily associated with delamination, particularly at the skin-stiffener interface, which may lead to a rapid degradation in structural integrity, as has been observed experimentally. This is a highly nonlinear problem that poses considerable difficulties in using neural networks. This work presents an FE-based optimization methodology for postbuckling stiffened panels that takes into account delamination. The optimization procedure uses a global–local modeling approach in the finite element package ABAQUS. The characteristics of this procedure and of the global and local models are discussed, with reference to an optimization conducted on the stacking sequence of several areas of an experimentally tested panel to improve its damage resistance in postbuckling. The ABAQUS analysis is validated by comparing the experimental and numerical buckling and postbuckling behavior of the original panel. The optimization problem was then formulated and a GA was used for the stacking-sequence optimization.

The GA was able to effectively find an optimized configuration for the stacking sequence of the panel flanges (and associated changes in the stiffener web and cap) to minimize the debonding between the skin and the stiffener for a specific load level. The initiation and progression of skin-stiffener debonding, as well as the buckling and postbuckling behavior, were compared with those of the nonoptimized design.

II. I-Stiffened Panel

A. Panel Description

The optimization procedure implemented in this work was applied to an I-stiffened panel [32] manufactured by BAE Systems. It was made using T300/914C unidirectional prepreg, and the nominal properties are shown in Table 1.

The manufactured panel was 604 mm wide and 850 mm long. The loaded edges were potted in a mixture of epoxy resin and fiberglass before being machined flat and parallel, resulting in an effective span of 790 mm. The panel was compression-tested under displacement control, with a crosshead displacement of 0.04 mm/ min. The out-of-plane displacements of the buckled skin were observed qualitatively using the shadow Moiré technique. Back-to-back strain gauges and linear voltage differential transducers (LVDTs) were arranged at various locations on the panel, as shown in Fig. 1a.

Table 1 Nominal material data

T300/914C unidirectional prepreg	
$E_{11\text{tension}}$	135 GPa
$E_{11\text{compression}}$	120 GPa
$E_{22\text{compression}}$	9 GPa
$E_{22\text{compression}}$	9 GPa
G_{12}	4.9 GPa
ν_{12}	0.28

The panel was reinforced by four evenly spaced stiffeners, secondarily bonded to the skin using FM300 adhesive. The stiffeners were 177 mm apart, as measured from their respective centerlines. The skin and stiffener cross section and layup are shown in Fig. 1b.

B. Experimental Results

The panel skin started to buckle at approximately 120 kN. At 160 kN, the first mode shape was fully visible, as shown in the Moiré fringe patterns in Fig. 2a, and was characterized by five half-waves in all three skin bays. The out-of-plane displacement at the panel's center, measured by LVDT A in Fig. 1a, is shown in Fig. 3a. Back-to-back strain gauges 3 and 4, mounted at the panel center and corresponding to the position of a buckle peak, indicate buckling at the critical load, as shown in Fig. 3b. At 244 kN, a mode switch from five to six half-waves in each of the skin bays was observed, as shown in Fig. 2b. The out-of-plane displacement in the panel center suddenly reduced, as did the longitudinal strains at the same position, because what was a node line switched to being close to an antinode line (Fig. 3). The mode jump was sudden, with an audible snap, and further cracking sounds occurred at 308, 361, and 416 kN, whereas a loud crack was heard at 444 kN, with three pops at 461 kN. Another mode shape change occurred in the left bay at 473 kN and in the right bay at 486 kN. This was another sudden jump from six to seven half-waves. The central half-wave remained in the six-half-wave configuration, but with the upper buckle being longer than the others, seemingly interacting with the buckles in the outer bays that appear squeezed at this position; Moiré fringe patterns in Fig. 2 illustrate this. More cracks were heard between 518 and 524 kN, and catastrophic failure occurred at a load of 525 kN.

In situ ultrasonic scans were conducted on the panel to try to understand the mechanisms of crack initiation and propagation that led to panel failure. A lot of experimental work has indicated that

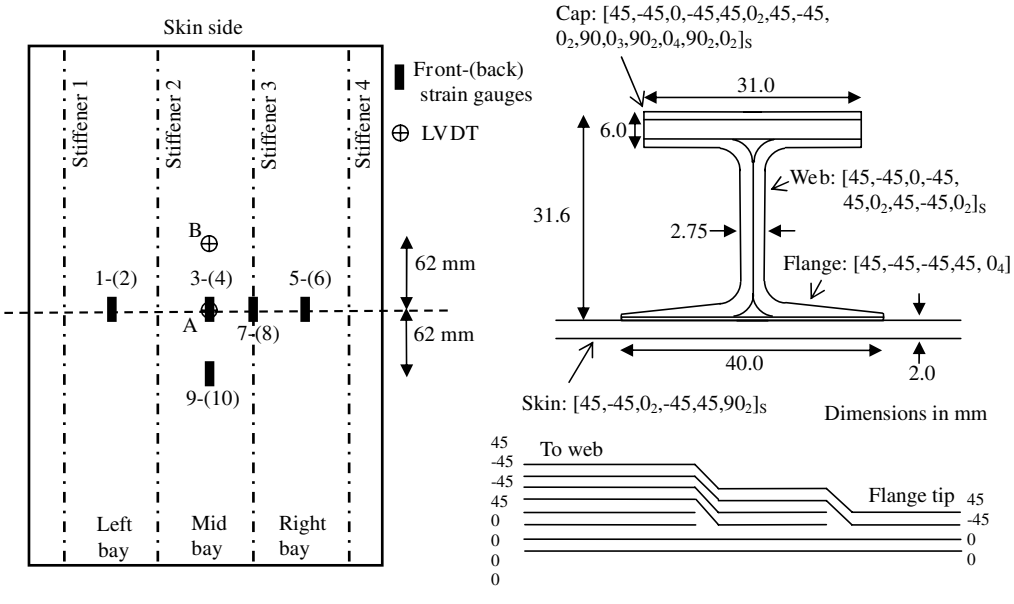

Fig. 1 I-stiffened panel experimental setup: a) positioning of back-to-back strain gauges and LVDTs and b) I-stiffener cross section and layup with flange dropoff detail.

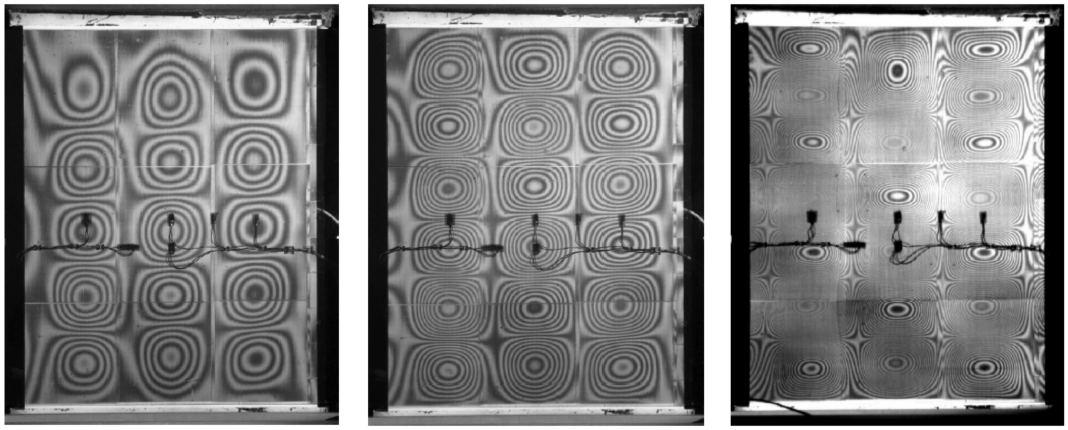

a) b) c)

Fig. 2 Moiré fringe patterns for I-stiffened panel at loading: a) 160 kN, b) 245 kN, and c) 487 kN.

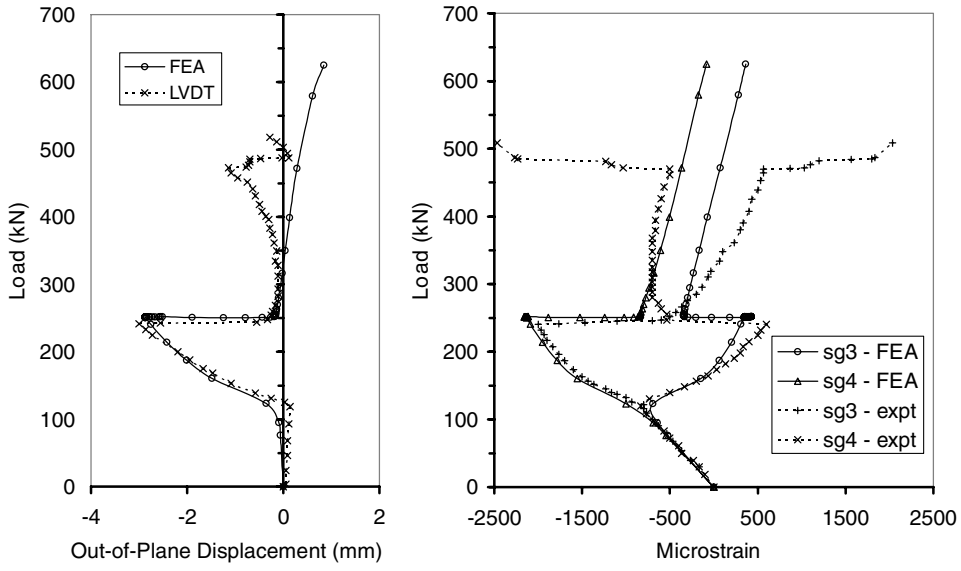

a) b)

Fig. 3 Experimental and numerical results for I-stiffened panel: a) out-of-plane displacements at I-stiffened panel center and b) strains at back-to-back strain gauges 3–4.

damage starts at the skin-stiffener interface at positions corresponding to buckle node and antinode lines, due to the stress concentrations in these regions [5–8]. Ultrasonic scans of the panel at antinode lines, in which transverse bending moment is a maximum, indicated possible delamination, but limitation of the ultrasound-scan procedure prevented accurate knowledge of failure initiation. Based on the features of the collapsed panel, a failure mechanism was suggested [32] that started with the delamination of the skin-stiffener interface underneath one of the stiffener webs. This caused the skin to buckle outward, peeling off the rest of the stiffener and, eventually, a second stiffener. This led to the whole panel bending away from the stiffener side and to eventual global collapse.

C. Finite Element Panel Model

A model of the experimental panel was developed using the FE package ABAQUS [33]. The model was meshed using 2800 four-node linear shell elements, with appropriate composite sections defined to represent the layup of the panel. Boundary conditions corresponding to the experimental configuration were imposed. Linear buckling analyses were conducted to find the buckling load and mode shapes of the panel. These were then used to introduce geometric imperfections into the panel to remove bifurcations and allow the ABAQUS nonlinear analysis algorithms to trace the full response of the panel in the postbuckling regime. A linear superposition of the first three buckling modes was used to impose an out-of-plane geometric imperfection, with a maximum out-of-plane displacement corresponding to 3% of the skin thickness. Because of the nonlinear and unstable nature of the response, the stabilize option available in ABAQUS was used in the analysis to aid convergence. This introduced volume-proportional damping by adding viscous forces to the global equilibrium equations. A value of 2% of the default damping factor suggested by the ABAQUS solver was used to ensure that the results were not adversely influenced.

D. Finite Element Analysis Results

The ABAQUS linear buckling analysis yielded a critical buckling load of 125.2 kN, in good agreement with the value of 120 kN obtained experimentally. The nonlinear finite element analysis model buckled into a five-half-wave configuration, as did the experimental panel. Good correlation was obtained between the out-of-plane displacements and strains at the panel center, as predicted by ABAQUS and by those obtained experimentally as the panel was loaded into its initial postbuckling region (Fig. 3). It should be noted, however, that the numerical and experimental panels buckled in opposite directions. For comparison purposes, the numerically predicted out-of-plane displacement at the panel center in Fig. 3a was made negative, but the central buckle crest actually buckled away from the stiffeners, rather than toward the stiffeners, as in the

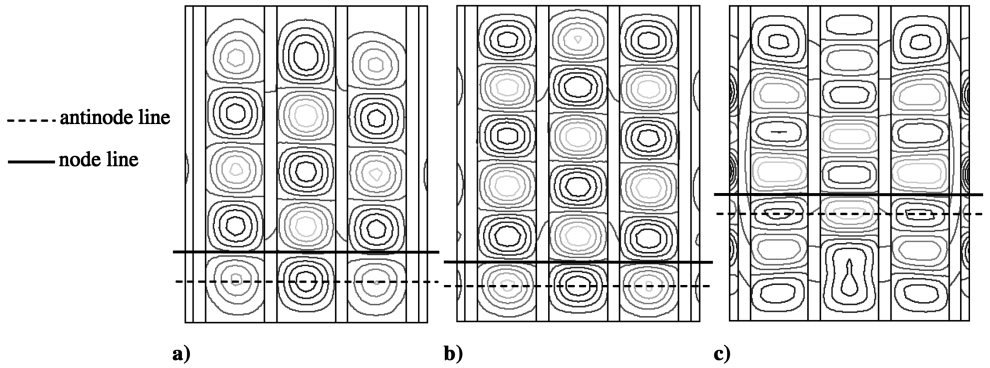

Fig. 4 Finite element out-of-plane displacements for I-stiffened panel at loading: a) 160 kN, b) 253 kN, and c) 800 kN.

experiment. This can be seen in the comparison of numerical and experimental strain gauge results in Fig. 3b. This variation may be due to the different initial imperfections between those present in the tested panel and those assumed for the finite element model.

The mode jump to six half-waves was captured by the FE analysis at a loading of about 251 kN, in very good agreement with the experimentally observed 244 kN. The second mode jump to seven half-waves occurred in the FE analysis at a loading past the collapse load of the experimental panel. Figure 4 shows the out-of-plane displacement contours for the ABAQUS model. The mode shapes are very similar to the experimental Moiré fringe patterns.

The use of static path-following finite element methods in ABAQUS showed that good quantitative and qualitative agreement in the results was obtained for buckling and postbuckling, whereas the second mode jump to seven half-waves, observed experimentally in the panel, was not captured by the FE analyses until a higher loading than that observed experimentally. This was due to the inevitable formation of microcracking at high loading, which was not taken into account in the FE model.

III. Skin-Stiffener Debonding Submodel

A. Panel Description

The use of shell elements in the global ABAQUS model meant that delamination at the skin-stiffener interface, which led to the failure of the I-stiffened panel, could not be captured. Hence, a detailed local model was created, which corresponded to a section of the stiffener and skin, chosen to analyze critical regions of the panel corresponding to buckle node and antinode lines. It had a length of 197.5 mm, width of 108.5 mm, and represented the central region of the panel at stiffener 2 in Fig. 1a. This global–local submodeling approach is shown in Fig. 5. The local model inherited the loading and boundary conditions from the results obtained in the global model. As the panel buckled and entered the postbuckling regime, displacements from the global-model solution automatically drove the local model.

The ABAQUS local model for the stiffener contained 1344 eight-node linear brick elements and 84 six-node triangular elements. It incorporated detailed geometric features that the global shell element model could not capture. These related to the termination schemes of the plies in the stiffener. The skin was modeled with 924 eight-node linear brick elements. Interface elements were introduced at the skin-stiffener interface.

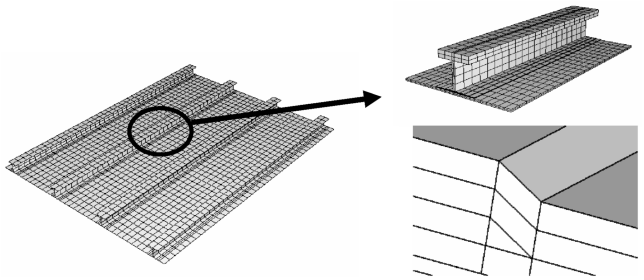

Fig. 5 Global–local modeling approach with flange drop detail in local model.

B. ABAQUS Interface Elements

Interface elements are interfacial decohesion elements placed between composite layers. They use failure criteria, combining aspects of strength-based analysis to predict the onset of softening at the interface on which the elements are placed, and fracture mechanics to predict the propagation of delamination. The traction-separation model in ABAQUS is based on damage-mechanics principles and involves an initially linear elastic behavior, followed by initiation and evolution of damage [34]. The traction-separation approach allows the combination of more than one damage mechanism to act at the same time on the cohesive interface, with each mechanism consisting of three components: damage initiation, damage evolution, and element removal. A traction-separation law is illustrated in Fig. 6 for mode I and modes II/III. A high initial stiffness holds the top and bottom faces together until point 1. For pure modes I, II, or III, once the interfacial normal and shear tractions reach their interlaminar tensile and shear strengths, respectively, at point 1, the stiffnesses are gradually reduced to zero via point 2 to point 3. For the ABAQUS model created, a quadratic nominal stress criterion was used for mixed-mode damage initiation, and a Benzeggagh–Kenane (BK) [35] fracture-energy-based criterion was used for mixed-mode damage evolution.

In ABAQUS, a damage level of 0 in a cohesive element indicates no damage and hence no debonding, and a level of 1 indicates that the stiffness in the cohesive element is completely degraded and full

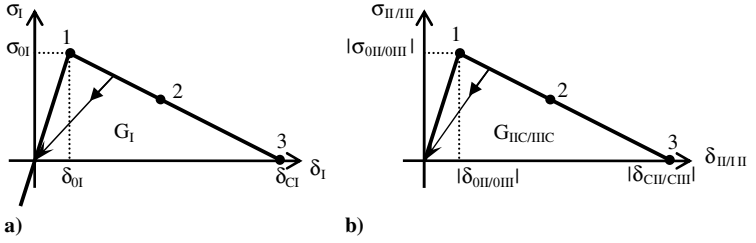

Fig. 6 Bilinear traction-separation laws for interface elements in a) mode-I delamination and b) modes-II/III delamination.

Table 2 Skin-stiffener interface bond properties

FM300 adhesive	
σ_{0I}	61.0 MPa
$\sigma_{0II}/\sigma_{0III}$	49.8 MPa
G_{IC}	532 J/m^2
G_{IIC}/G_{IIIC}	2358 J/m^2
Film thickness	0.13 mm
ν_{12}	0.28

debonding has occurred. The cohesive zone between the stiffener and skin in the local model was discretized using a single layer of 336 cohesive elements. Properties relating to the skin-stiffener interface, secondarily bonded using FM300 adhesive, were taken from experimental values [36] and are shown in Table 2. These properties were used in ABAQUS to define damage initiation and propagation of delamination using the cohesive elements.

Before running the local model, mesh sensitivity and viscosity parameter tests were conducted. The mesh described here was deemed appropriate, because no great variations in subsequent debonding results were observed when a finer mesh was used. The viscosity parameter was set to 0.001 after a parametric study was conducted. This relates to an ABAQUS relaxation factor that aids in overcoming the convergence problems often associated with cohesive elements [35]. A higher value will speed up convergence and hence reduce computational cost, but may lead to erratic results.

C. Local-Model Finite Element Analysis Results

The local model allowed investigation of the damage in the skin-stiffener interface as the panel was loaded in both its prebuckling and postbuckling fields. Figure 7 shows the deformed shape of the local model at various loads, with a deformed shape scaling factor of 5. The deformed shape is shown for the same loads as for the global-model displacement contours in Fig. 4 and at an additional loading of 500 kN. At a load of 160 kN, the panel had buckled and showed the five-half-wave configuration. The buckle node and antinode lines are clearly visible in Fig. 7a. As the load was increased, the panel mode jumped at 251 kN from the five-half-wave configuration to a six-half-wave configuration, shown in Fig. 7b. As the loading was increased to 500 kN, the buckle crests grew in magnitude, as is visible in Fig. 7c. Figure 7d shows the features of the ABAQUS local model after the mode jump to seven half-waves.

The degradation of the cohesive elements at the skin-stiffener interface, as a response to the buckling and postbuckling behavior of the panel, was investigated. Figure 8 shows the stiffness degradation of the elements at various loads. In the five-half-wave configurations at a load of 160 kN, there was very little degradation in the cohesive elements. As the loading was increased and the buckle crests grew in magnitude, the elements directly under the stiffener web started to degrade at a position corresponding to an antinode line. This agreed with experimental results [8], which indicated that at an antinode line, the moment transfer between the stiffener web and stiffener flange/panel skin acted to pull the flange away from the panel. As the loading increased, so did the stiffness degradation of the interface elements. At the mode jump to six half-waves, the position of the node and antinode lines changed. As a result, so did the extent of the debonding, as is visible in Fig. 8b. The position of the new antinode line resulted in more stiffness degradation at this location. This degradation increased with increasing loading, shown in Fig. 8c. For very high loads in the model, the whole interface was shown to be almost completely debonded (Fig. 8d).

IV. Formulation of the Optimization Problem

An optimization strategy was formulated to find the best stacking sequence in the I-stiffened panel flanges, to increase damage resistance of the panel in postbuckling. The problem was defined as a minimization of the sum of the total damage in all the cohesive elements at the skin-stiffener interface at a specific load. Because the panel was tested under displacement control, a maximum end displacement of 2.8 mm was chosen, because this is past the critical buckling load of the panel and in its postbuckling regime. Calculation of the objective function required the global-model buckling analysis to find the buckling load and mode shapes, the global nonlinear analysis to trace the panel's buckling and postbuckling responses using the buckle analysis results to introduce geometric imperfections, and the local-model analysis to model the skin-stiffener debonding. The panel flanges contained eight plies, as illustrated in Fig. 1b. In the optimization, these plies were limited to orientations of 0, 45, −45, and 90 deg, commonly used in industry. The way in which the panel was manufactured meant that most of the plies in the flanges were continued into the stiffener web and cap. Hence, changes in ply orientation in the flanges resulted in changes in the stacking sequence in the rest of the stiffener. This was accounted for by automatically modifying the ABAQUS input files in response to the flange's stacking-sequence alterations. The stacking sequence was defined in terms of four variables, known as ply-orientation-identity variables [37]. Each of these variables represented one of the four possible orientations and assumed a value of 1 if a specific ply

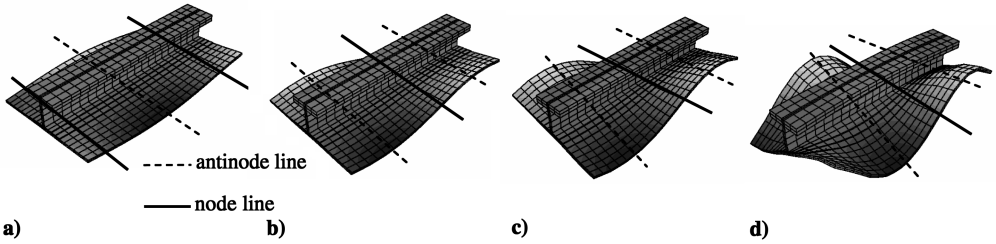

Fig. 7 Local model deformed shape at loading: a) 160 kN, b) 253 kN, c) 500 kN, and d) 800 kN.

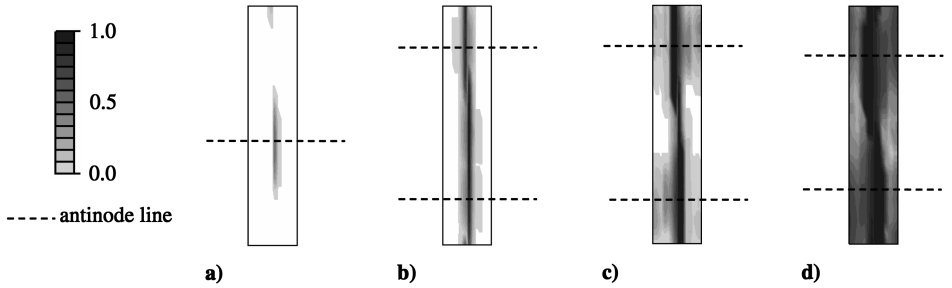

Fig. 8 Cohesive element damage in skin/stiffener interface at loading: a) 160 kN, b) 253 kN, c) 500 kN, and d) 800 kN.

was oriented in that direction and a value of 0 otherwise. The plies were numbered using the index i, which took the values of $i = 1, \ldots, 8$, where eight is the number of plies in the panel flanges. Adopting this formulation, the optimization problem was stated as follows:

Find o_i, n_i, f_i^p, and f_i^m for $i = 1, \ldots, 8$.

To minimize

$$\sum_{j=1}^{\text{elements}} SDEG$$

Such that $o_i + n_i + f_i^p + f_i^m = 1$ for $i = 1, \ldots, 8$ (ply-identity constraint), where "elements" are the total number of cohesive elements in the local model and $SDEG$ is the damage variable (0–1) associated with each element. Because of the discrete nature of the problem, a GA was constructed in MATLAB [38] to run the optimization.

V. Genetic Algorithm

A. Initial Population

The implemented GA worked with a fixed-size population, represented by a matrix. The number of columns in the matrix corresponded to the number of individuals, and the number of rows corresponded to the number of varying plies (in this case, eight). The initial population was created randomly, each element of the matrix being an integer in the range of one to four, with each integer corresponding to one of the ply orientations and following the ply-orientation-identity chromosome-string representation.

B. Fitness Calculation

The chromosome string was first decoded to the real flange orientations, and the ABAQUS model was updated to represent the appropriate layup. The global buckling and nonlinear analyses were run, followed by the local debonding analysis to calculate the objective function for the individual. The GA then assigned a fitness value to each individual. A rank-based fitness with a selective pressure of two was used, meaning that the individual with the lowest objective function was assigned a fitness of two, the one with the highest objective function was assigned a fitness of zero, and all other individuals were linearly assigned values between the two.

C. Selection

Individuals for breeding were selected using stochastic universal sampling. Each individual was mapped to a segment of a line representing the whole population, with the length of each segment proportional to the individual's fitness. Equidistant pointers were then created for the number of individuals to be selected. The position of the pointers along the line determined the individuals selected.

D. Crossover

Selected individuals were then bred by the GA using two-point crossover. Two-point crossover works by selecting two randomly placed cutoff points in each individual's string and then swapping information between two individuals to create the offspring, as shown in Table 3.

E. Mutation

After crossover, the GA applied mutation to the generated offspring. Mutation acts to prevent the loss of potentially favorable genetic traits and allows the crossover operator to remain effective even in the latter stages of the optimization. The mutation applied changed a random bit in each individual's string, with a probability of $1/N$, where N was the number of bits in the individual's string.

Table 3 Two-point crossover strings

Parent 1: 21/23134/1	Parent 2: 31/24321/4
Offspring 1: 21/24321/1	Offspring 2: 31/23134/4

F. Reinsertion

A fitness-based reinsertion method was implemented to reinsert offspring into the population. This took all the created offspring and replaced the least-fit members of the population, keeping the population size constant from generation to generation.

G. Termination

A maximum number of 20 generations was set to stop the algorithm if an optimum solution was not found. However, a flag was implemented so that if a number of successive individuals have the same genetic string, then the user is alerted that the algorithm has converged.

H. GA Verification

To find appropriate values for the various genetic parameters and validate the GA, a simple plate-buckling-load optimization problem, first proposed by Hafta and Walsh [39], was used. The aim was to find the optimal stacking sequence for a symmetric 16-laminate plate subject to various biaxial loads, to maximize the buckling load. The symmetric layup meant that each individual had eight bits in its chromosome string, as in the panel optimization, and ABAQUS was used in the buckling-load evaluations. The GA was able to find optimal designs and the results matched those by Hafta and Walsh. It was seen that a population size of 40 was appropriate, and hence the same value was used for the panel optimization. Similarly, the value for the generation gap (the percentage of individuals to be selected for breeding) was set to 0.95, and the probability of crossover was set to 0.7. These values were then used in the stiffened-panel optimization.

I. Reduction of Computational Effort

To reduce computational costs, the GA was modified to avoid identical function evaluations. To do this, all the information relating to each function evaluation was stored in a file. As the GA progressed and was about to evaluate an individual, the file was scanned. If the particular individual had already been evaluated, then the same objective function was used, therefore not requiring a new function evaluation. This helped to significantly reduce computational time, especially in the latter generations, in which the GA was converging to the optimum and most of the individuals in the population had already appeared in previous generations.

VI. Optimization Results

A. GA Results

The GA showed convergent results after 18 iterations. The optimized-panel design consisted of a flange layup of $[0_3, 45, -45, 0, 90_2]$. This and the corresponding changes in layup in the remaining sections of the stiffener are illustrated in Table 4.

The ABAQUS buckling analysis gave a buckling load for the optimized design of 115.9 kN. This was 7.4% lower than the nonoptimized design ABAQUS buckling load of 125.2 kN. The prebuckling stiffness of the optimized panel was 190.1 kN/mm, compared with 190.3 kN/mm for the nonoptimized design, or 0.2% lower. The postbuckling stiffness was 1.6% lower, at 154.6 kN/mm, compared with 157.1 kN/mm. The objective function of the optimum design was 45.2, corresponding to the sum of the ABAQUS

Table 4 Layup of optimized design

	Layup
Skin	$[45, -45, 0_2, -45, 45, 90_2]_S$
Flange	$[0_3, 45, -45, 0, 90_2]$
Web	$[0_4, 45, -45, 0, 45, -45, 90_2]_S$
Cap	$[0_4, 45, -45, 0, 45, -45, 90_3, 0_3, 90_2, 0_4, 90_2, 0_2]S$

Table 5 Comparison of optimized and nonoptimized configurations

	Nonoptimized	Optimized	% difference
Flange layup	$[45, -45, -45, 45, 0_4]$	$[0_3, 45, -45, 0, 90_2]$	
Buckling load, kN	125.2	115.9	−7.4%
Prebuckling stiffness, kN/mm	190.3	190.1	−0.2%
Postbuckling stiffness, kN/mm	157.1	154.6	−1.6%
Cohesive element damage	77.8	45.2	−41.9%

damage variable in all the cohesive elements at the skin-stiffener interface for the applied end-displacement loading of 2.8 mm. This was 41.9% lower than the 77.8 value of the nonoptimized design. These results are summarized in Table 5.

B. Optimized-Panel Global-Model Results

Following buckling, the optimized panel adopted a five-half-wave configuration, just as with the nonoptimized panel, as shown in Fig. 9a. The buckle crests grew in size, as illustrated in Fig. 9b, and jumped to a six-half-wave configuration at a higher load than that in the nonoptimized panel. The mode jump for the optimized configuration was predicted to occur at 457 kN, compared with 240 kN in the nonoptimized panel. A further mode jump to seven half-waves, not shown in Fig. 9, took place at 726 kN.

C. Optimized-Panel Local-Model Results

Figure 10 shows the stiffness degradation in the cohesive elements at increasing load. As in the nonoptimized case, degradation began at a position corresponding to an antinode line. As loading increased and the buckle crests deepened, the elements degraded further. What is visible from Figs. 8a and 10a is that for elements on the side on which the skin has a tendency to peel off, the flanges degraded more than for elements on the side on which the buckle shapes pushed the skin toward the stiffener. In Fig. 8b, the nonoptimized-panel mode had jumped, but not the optimized panel in Fig. 10b. As a result, the cohesive element degradation was still concentrated toward the submodel center, because this was still the location of the antinode. What is apparent is that much less damage is visible for this load level in the optimized panel in Fig. 10b compared with the nonoptimized design in Fig. 8b. When the mode jump occurred at the higher loading of 457 kN, then the cohesive element degradation spread across the length of the interface, due to the relocation of the node lines, as shown in Fig. 10c. At a higher load, as shown in Fig. 10d, most interface elements had completely failed.

Figure 10 shows that the delay in the mode jump from five to six half-waves, as a result of the change in layup, meant that element degradation spread later across the length of the skin-stiffener interface. The total damage in the cohesive elements in the postbuckling regime at which the optimization is conducted was reduced by 41.9% as a result of the optimization process.

D. Optimization Considerations

The results show that the GA found a new layup for the panel's I-stiffener flanges to decrease the predicted level of skin-stiffener debonding. This decrease for the optimized design was accompanied by only modest decreases in buckling load, prebuckling, and postbuckling stiffnesses. Table 5 indicates that the drops in prebuckling and postbuckling stiffnesses are just 0.2 and 1.6%, respectively, and 7.4% in the initial buckling load. Constraints may be included in the GA, specifying minimum thresholds for these values.

Monitoring of the GA allowed several observations to be made relating to the effect of changes in the flange layup on the successive level of debonding displayed by the design. What is interesting to note is that the optimized design has three 0-deg-oriented plies at the top of the flanges, away from the skin-stiffener interface. Changes in their orientations away from the final configuration typically led to

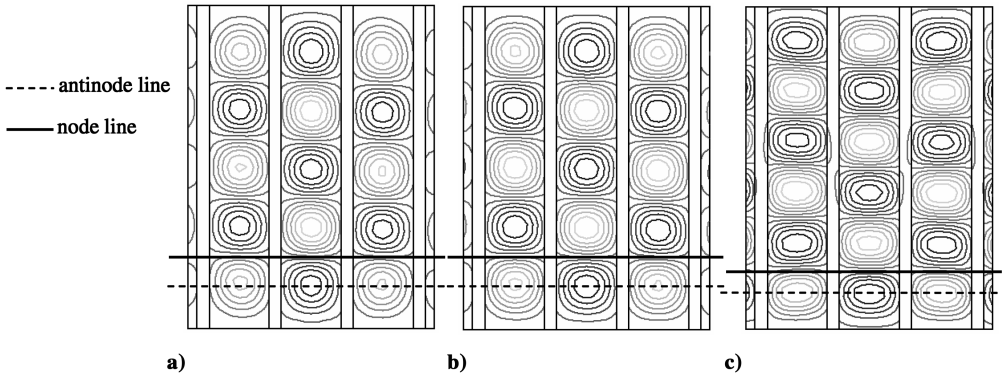

Fig. 9 Finite element out-of-plane displacements for optimized panel at loading: a) 160 kN, b) 253 kN, and c) 500 kN.

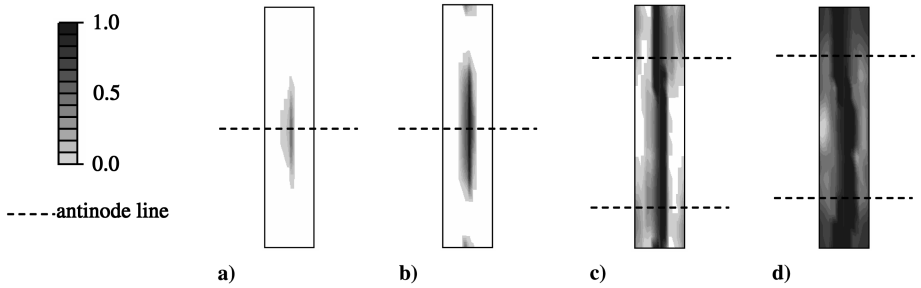

Fig. 10 Cohesive element damage for optimized panel in skin/stiffener interface at loading: a) 160 kN, b) 253 kN, c) 500 kN, and d) 870 kN.

greater changes in the total damage at the interface than changes in the other five plies. For instance, the optimized design had a flange layup of $[0_3, 45, -45, 0, 90_2]$. Comparing this with the slightly different design of $[0_2, 45_2, -45, 0, 90_2]$, in which just one of the three 0-deg-oriented plies on the outside of the flanges becomes a 45-deg ply, shows the damage increasing from 45.2 to 83.4, indicating the sensitivity of the panel behavior to specific changes in its layup. Hence, the GA did fulfill its task of finding an optimized configuration to reduce the FE-predicted debonding of the skin and stiffener and also gave insight into how some of the changes in the stacking-sequence influence the panel behavior.

VII. Conclusions

A global–local modeling approach was presented in which an I-stiffened panel was modeled using the finite element package ABAQUS. A global model using shell elements was created and its accuracy in predicting the buckling and postbuckling responses of the I-stiffened panel was assessed. This included a linear eigenvalue analysis, for which the predicted buckling load was in good agreement with that observed experimentally. Results from the buckling analyses were then used to introduce geometric imperfections to allow ABAQUS nonlinear algorithms to trace the panel's postbuckling response. Comparisons of the FE nonlinear analysis compared qualitatively well with the experimental ones, and good quantitative agreement in the strains and out-of-plane displacements was found in the panel's postbuckling regime. A local model of solid elements representing the skin and stiffener, with cohesive elements capable of modeling the debonding at the skin-stiffener interface, was then set up and directly driven by the solution of the global model.

An optimization procedure was linked to local and global models to change the stacking sequence in the panel flanges, to minimize the extent of skin-stiffener debonding. The objective function was defined as the sum of the stiffness degradation of all the cohesive elements placed at the skin-stiffener interface. Because of the discrete nature of the problem, a GA was used with ply-orientation-identity variables. The GA linked to the global and local models and provided an automated optimization scheme that resulted in a revised flange layup. The buckling and postbuckling behavior of the optimized panel were compared with those of the nonoptimized one, and the buckling load, prebuckling stiffness, and postbuckling stiffness were found to be 7.4, 0.2, and 1.6% lower, respectively. For an applied end displacement of 2.8 mm, corresponding to a load of approximately 450 kN, the optimized panel showed a total interface damage of 41.9% less than the nonoptimized case.

This optimization proof of concept could easily be extended to change the layup of other portions of the panel. Constraints on factors such as buckling load, prebuckling stiffness, and postbuckling stiffness could be added to obtain designs that satisfy other design parameters. Additionally, other panel configurations could be considered or factors such as changes in stiffener geometries could be incorporated into the design variables themselves.

References

[1] Romeo, G., "Experimental Investigation on Advanced Composite-Stiffened Structures Under Uniaxial Compression and Bending," *AIAA Journal*, Vol. 24, No. 11, 1986, pp. 1823–1830.

[2] Starnes, J. H., Jr., Knight, N. F., Jr., and Rouse, M., "Postbuckling Behavior of Selected Flat Stiffened Graphite-Epoxy Panels Loaded in Compression," *AIAA Journal*, Vol. 23, No. 8, 1985, pp. 1236–1246.

[3] Bauld, N. R., Jr., and Khot, N. S., "A Numerical and Experimental Investigation of the Buckling Behavior of Composite Panels," *Computers and Structures*, Vol. 15, No. 4, 1981, pp. 393–403.

[4] Nemeth, M. P., *Buckling and Postbuckling Behavior of Laminated Composite Plates with a Cutout*, NASA, Hampton, VA, 1996.

[5] Falzon, B. G., Stevens, K. A., and Davies, G. A. O., "Postbuckling Behavior of a Blade-Stiffened Composite Panel Loaded in Uniaxial Compression," *Composites, Part A: Applied Science and Manufacturing*, Vol. 31, No. 5, 2000, pp. 459–468.

[6] Falzon, B. G., and Stevens, G. P., "Buckling Mode Transition in Hat-Stiffened Composite Panels Loaded in Uniaxial Compression," *Composite Structures*, Vol. 37, No. 2, 1997, pp. 253–267.

[7] Falzon, B. G., "The Behavior of Damage Tolerant Hat-Stiffened Composite Panels Loaded in Uniaxial Compression," *Composites, Part A: Applied Science and Manufacturing*, Vol. 32, No. 9, 2001, pp. 1255–1262.

[8] Stevens, K. A., Ricci, R., and Davies, G. A. O., "Buckling and Postbuckling of Composite Structures," *Composite Structures*, Vol. 26, No. 3, 1995, pp. 189–199.

[9] Kong, C., Lee, I. C., Kim, C. G., and Hong, C. S., "Postbuckling and Failure of Stiffened Composite Panels Under Axial Compression," *Composite Structures*, Vol. 42, No. 1, 1998, pp. 13–21.

[10] Adali, S., Richter, A., Verijenko, V. E., and Summers, E. B., "Optimal Design of Hybrid Laminates with Discrete Ply Angles for Maximum Buckling Load and Minimum Cost," *Composite Structures*, Vol. 32, Nos. 1–4, 1995, pp. 409–415.

[11] Adali, S., Walker, M., and Verijenko, V. E., "Multi-Objective Optimization of Laminated Plates for Maximum Prebuckling, Buckling and Postbuckling Strength Using Continuous and Discrete Ply Angles," *Composite Structures*, Vol. 35, No. 1, 1996, pp. 117–130.

[12] Adali, S., Lene, F., Duvaut, G., and Chiaruttini, V., "Optimization of Laminated Composites Subject to Uncertain Buckling Loads," *Composite Structures*, Vol. 62, Nos. 3–4, 2003, pp. 261–269.

[13] Chai, G. B., Ooi, K. T., and Khong, P. W., "Buckling Strength Optimization of Laminated Composite Plates," *Computers and Structures*, Vol. 46, No. 1, 1993, pp. 77–82.

[14] Walker, M., Adali, S., and Verijenko, V. E., "Optimal Design of Symmetric Angle-Ply Laminates Subject to Nonuniform Buckling Loads and In-Plane Restraints," *Thin Walled Structures*, Vol. 26, No. 1, 1996, pp. 45–60.

[15] Walker, M., Adali, S., and Verijenko, V. E., "Optimization of Symmetric Laminates for Maximum Buckling Load Including the Effects of Bending-Twisting Coupling," *Computers and Structures*, Vol. 58, No. 2, 1996, pp. 313–319.

[16] Walker, M., and Reiss, T., "Application of Mathematica to the Optimal Design of Composite Shells for Improved Buckling Strength," *Engineering Computations*, Vol. 15, No. 2, 1998, pp. 260–267.

[17] Walker, M., "Optimal Design of Symmetric Laminates With Cutouts for Maximum Buckling Load," *Computers and Structures*, Vol. 70, No. 3, 1999, pp. 337–343.

[18] Fukunaga, H., Sekine, H., Sato, M., and Iino, A., "Buckling Design of Symmetrically Laminated Plates Using Lamination Parameters," *Computers and Structures*, Vol. 57, No. 4, 1995, pp. 643–649.

[19] Bushnell, D., "Optimization of Composite, Stiffened, Imperfect Panels Under Combined Loads for Service in the Postbuckling Regime," *Computer Methods in Applied Mechanics and Engineering*, Vol. 103, Nos. 1–2, 1993, pp. 43–114.

[20] Goldberg, D. E., *Genetic Algorithms in Search, Optimization, and Machine Learning*, 1st ed., Addison–Wesley, London, 1989.

[21] Le Riche, R., and Haftka, R. T., "Optimization of Laminate Stacking Sequence for Buckling Load Maximization by Genetic Algorithm," *AIAA Journal*, Vol. 31, No. 5, 1993, pp. 951–970.

[22] Le Riche, R., and Haftka, R. T., "Improved Genetic Algorithm for Minimum Thickness Composite Laminate Design," *Composites Engineering*, Vol. 5, No. 2, 1994, pp. 143–161.

[23] Kogiso, N., Watson, L. T., Gurdal, Z., Hafta, R. T., and Nagendra, S., "Minimum Thickness Design of Composite Laminates Subject to Buckling Strength Constraints by Genetic Algorithm," *Mechanics of Composite Materials and Structures*, Vol. 1, No. 1, 1994, pp. 95–117.

[24] Kang, J., and Chun-gon, K., "Minimum-Weight Design of Compressively Loaded Composite Plates and Stiffened Panels for Postbuckling Strength by Genetic Algorithm," *Composite Structures*, Vol. 69, No. 2, 2005, pp. 239–246.

[25] Nagendra, S., Jestin, D., Gurdal, Z., Hafta, R. T., and Watson, L. T., "Improved Genetic Algorithm for the Design of Stiffened Composite Panels," *Computers and Structures*, Vol. 58, No. 3, 1996, pp. 543–555.

[26] Gantovnik, V. B., Gurdal, Z., and Watson, L. T., "A Genetic Algorithm with Memory for Optimal Design of Laminated Sandwich Composite Panels," *Composite Structures*, Vol. 58, No. 4, 2002, pp. 513–520.

[27] Gantovnik, V. B., Anderson-Cook, C. M., Gurdal, Z., and Watson, L. T., "A Genetic Algorithm with Memory for Mixed Discrete-Continuous Design Optimization," *Computers and Structures*, Vol. 81, No. 20, 2003, pp. 2003–2009.

[28] Lin, C.-C., and Lee, Y.-J., "Stacking Sequence Optimization of Laminated Composite Structures Using Genetic Algorithm with Local Improvement," *Composite Structures*, Vol. 63, Nos. 3–4, 2004, pp. 339–345.

[29] Di Sciuva, M., Gherlone, M., and Lomario, D., "Multiconstrained Optimization of Laminated and Sandwich Plates Using Evolutionary Algorithms and Higher-Order Plate Theories," *Composite Structures*, Vol. 59, No. 1, 2003, pp. 149–154.
[30] Bisagni, C., and Lanzi, L., "Post-Buckling Optimization of Composite Stiffened Panels Using Neural Networks," *Composite Structures*, Vol. 58, No. 2, 2002, pp. 237–247.
[31] Lanzi, L., and Bisagni, C., "Minimum Weight Optimization of Composite Stiffened Panels Using Neural Networks," 44th AIAA/ASME/ASCE.AHS Structures, Structural Dynamics, and Materials Conference, Norfolk, VA, AIAA Paper 2003-1698, 2003.
[32] Cerini, M., "Investigation of Secondary Instabilities in Postbuckling Stiffened Composite Structures," Ph.D., Thesis, Department of Aeronautics, Imperial College London, London, 2005.
[33] ABAQUS, Finite Element Package, Ver. 6.5, ABAQUS. Inc., Providence, RI, 2005.
[34] Camanho, P. P., and Davila, C. G., "Mixed-Mode Decohesion Finite Elements for the Simulation of Delamination in Composite Materials," NASA TP 211737, 2002.
[35] "ABAQUS Version 6.5 Documentation," 1st ed., ABAQUS. Inc., Providence, RI, 2004.
[36] "Skin/Stringer Interface Bond: Mode I and Mode II Fracture Toughness Tests," National Physics Lab., Teddington, England, U.K., 1999.
[37] Gurdal, Z., Hafta, R. T., and Hajela, P., *Design and Optimization of Laminated Composite Materials*, 1st ed., Wiley, New York, 1999.
[38] MATLAB, Software Package, Ver. 6, Mathworks, Natick, MA, 2001.
[39] Hafta, R. T., and Walsh, J. L., "Stacking-Sequence Optimization for Buckling of Laminated Plates by Integer Programming," *AIAA Journal*, Vol. 30, No. 3, 1992, pp. 814–819.

A. Roy
Associate Editor